AGU PUBLICATIONS

JGR

Journal of Geophysical Research: Atmospheres

RESEARCH ARTICLE
10.1002/2016JD025502

Key Points:
- The relationship of North Pacific SLP anomalies to subsequent ENSO events depends on the state of simultaneous South Pacific SLP anomalies
- The influence of North Pacific SLP anomalies on the westerly along the equator interferes with the effect of South Pacific anomalies
- A model based on combined North and South Pacific signals significantly improves the forecast skill of ENSO 1 year ahead

Supporting Information:
- Supporting Information S1

Correspondence to:
R. Ding,
drq@mail.iap.ac.cn

Citation:
Ding, R., J. Li, Y.-h. Tseng, C. Sun, and F. Xie (2017), Joint impact of North and South Pacific extratropical atmospheric variability on the onset of ENSO events, *J. Geophys. Res. Atmos.*, *122*, 279–298, doi:10.1002/2016JD025502.

Received 12 JUN 2016
Accepted 22 DEC 2016
Accepted article online 23 DEC 2016
Published online 14 JAN 2017

Joint impact of North and South Pacific extratropical atmospheric variability on the onset of ENSO events

Ruiqiang Ding[1,2], Jianping Li[3], Yu-heng Tseng[4], Cheng Sun[3], and Fei Xie[3]

[1]State Key Laboratory of Numerical Modeling for Atmospheric Sciences and Geophysical Fluid Dynamics (LASG), Institute of Atmospheric Physics, Chinese Academy of Sciences, Beijing, China, [2]Plateau Atmosphere and Environment Key Laboratory of Sichuan Province, Chengdu University of Information Technology, Chengdu, China, [3]College of Global Change and Earth System Sciences (GCESS), Beijing Normal University, Beijing, China, [4]Climate and Global Dynamics Division, NCAR, Boulder, Colorado, USA

Abstract Previous studies have indicated that boreal winter subtropical and extratropical sea surface pressure (SLP) anomalies over both the North and South Pacific are significantly related to the El Niño–Southern Oscillation (ENSO) state in the following boreal winter. Here we use observational data and model simulations to show that the ability of the boreal winter North Pacific SLP anomalies to initiate ENSO events a year later may strongly depend on the state of the simultaneous South Pacific SLP anomalies and vice versa. When the boreal winter North Pacific SLP anomalies are of the opposite sign to the simultaneous South Pacific anomalies, the correlation of the North or South Pacific anomalies with the following ENSO state becomes much weaker, and the strength of the ENSO events also tends to be weaker. One possible reason for this is that when the boreal winter North and South Pacific SLP anomalies have the opposite sign, the westerly anomalies over the western-central equatorial Pacific during the following boreal summer are greatly reduced by the interference between the antecedent North and South Pacific SLP anomalies, thereby not favoring the development of ENSO events. Further analysis indicates that a combination of North and South Pacific precursor signals may serve to enhance the ENSO prediction skill.

1. Introduction

The El Niño–Southern Oscillation (ENSO) is the dominant climate fluctuation in the tropical Pacific over seasonal to interannual time scales and has substantial effects on climate around the world. Over recent decades, significant advances have been made in our understanding of ENSO, and it is generally accepted that the development of ENSO events involves a positive feedback between the intensity of the trade winds and zonal contrasts in sea surface temperature (SST); i.e., the Bjerknes feedback [*Bjerknes*, 1969]. Previous studies have suggested that higher-frequency atmospheric variability over the western-central equatorial Pacific, such as the Westerly Wind Events (WWEs) [*McPhaden et al*., 1992; *McPhaden*, 1999] and Madden–Julian Oscillation (MJO) [*Madden and Julian*, 1994], can act as a trigger of the Bjerknes feedback. In addition, observational and modeling studies have suggested that atmospheric variability originating outside the tropical Pacific also has a significant impact on the onset of ENSO, including the effects of extratropical atmospheric variability over the North Pacific [*Vimont et al*., 2003a, 2003b, 2009; *Anderson*, 2003; *Anderson and Maloney*, 2006; *Alexander et al*., 2010; *Yu et al*., 2010; *Yu and Kim*, 2011; *Ding et al*., 2015a], over the South Pacific [*Jin and Kirtman*, 2009; *Terray*, 2011; *Hong et al*., 2014; *Zhang et al*., 2014a; *Ding et al*., 2015b], and over the Southern Indian/Atlantic Oceans [*Terray*, 2011]. Fluctuations in these extratropical atmospheric patterns have been found to be useful as precursors for ENSO events [*Vimont et al*., 2003a; *Anderson*, 2003; *Terray*, 2011; *Larson and Kirtman*, 2014; *Ding et al*., 2015b].

Given that both the North and South Pacific extratropical atmospheric variability exert influence on subsequent ENSO events, the question arises as to whether the North Pacific influence on ENSO interferes with the impact of the South Pacific. The aforementioned studies focused mainly on the individual influence of the North and South Pacific atmospheric variability on ENSO events, rather than their joint role. In contrast, this paper will focus on the joint effect of this North and South Pacific extratropical atmospheric variability on subsequent ENSO events. The rest of the paper is organized as follows. Section 2 describes the observations, model data sets, and the analysis method used in this study. Section 3 examines the joint relationship between the tropical Pacific SST anomalies and antecedent North and South Pacific atmospheric variability in both observations and numerical simulations. Our findings are summarized and discussed in section 4.

2. Observations, Model Data Sets, and the Analysis Method

2.1. Observational Data Sets

We use the SST field from the National Oceanic and Atmospheric Administration (NOAA) Extended Reconstructed SST version 3b data set (ERSSTv3b) [*Smith et al*., 2008]. We use atmospheric fields from the National Centers for Environmental Prediction-National Center for Atmospheric Research (NCEP-NCAR) reanalysis (NCEP1) data set [*Kalnay et al*., 1996]. The NCEP1 data set includes surface wind and sea level pressure (SLP) fields. The monthly anomalies are obtained by removing the climatological (1981–2010) mean annual cycle and linear trends. Our analysis mainly focused on the period 1948–2015, because both the ERSST and NCEP1 data sets were available for this time span. To validate the results obtained from the NCEP1 data set, we also use the latest reanalysis data sets including the NCEP-Department of Energy Reanalysis 2 (NCEP2) [*Kanamitsu et al*., 2002] and the ECMWF (European Centre for Medium-Range Weather Forecasts) Interim Reanalysis (ERA-Interim) [*Dee et al*., 2011] over the period 1979–2015.

2.2. Model Data Sets

To evaluate if the current coupled models can reproduce the joint relationship between the tropical Pacific SST anomalies and antecedent North and South Pacific atmospheric variability, we use the historical simulations of the large ensemble with the fully coupled Community Earth System Model 1 (CESM1), hereafter CESM-LE. CESM1 consists of coupled atmosphere (Community Atmosphere Model version 5 (CAM5), 30 vertical levels), ocean (Parallel Ocean Program version 2 (POP2), 60 vertical levels), land (Community Land Model version 4 (CLM4)), and sea ice (Los Alamos Sea Ice Model version 4 (CICE4)) component models. The CESM-LE historical simulations are an ensemble of 30 simulations from 1920 to 2005 at approximately 1° horizontal resolution in all model components. In CESM-LE, each simulation began with a 1500 year control simulation under constant preindustrial (year 1850) forcing and was then forced with the same historical greenhouse gases and aerosol emissions (up to 2005) but starting from a slightly different initial atmospheric state (created by randomly perturbing temperatures at the level of round-off error). Details of the CESM-LE simulations may be found in *Kay et al*. [2015].

To further investigate the role of internal variability in the joint relationship of the antecedent North and South Pacific atmospheric variability to ENSO, we use the preindustrial control (piControl) simulations of CESM and the Community Climate System Model version 4 (CCSM4). CCSM4 is a fully coupled model of the earth's physical climate system, which is made up of coupled atmosphere (CAM4, 26 vertical levels), ocean (POP2, 60 vertical levels), land (CLM4), and sea ice (CICE4) component models. A general description of CCSM4 is given in *Gent et al*. [2011]. In the piControl simulation, CCSM4 is configured at nominal 1° latitude-longitude resolution with external forcings fixed at 1850. The CCSM4 (CESM) piControl simulation spans 1300 (1500) model years, but only a 501 year segment between model years 800 and 1300 (1000 and 1500) is used in the present analysis, in order to avoid the initial adjustment period due to the model spin-up process [*Danabasoglu et al*., 2012].

2.3. Statistical Methods

We primarily employ correlation and regression analysis to study the relationship between ENSO and antecedent North and South Pacific atmospheric variability. The significance of correlation and regression coefficients is determined using a two-tailed Student's *t* test. For the correlations between variables *x* and *y*, the effective number of degrees of freedom N_{eff} is determined via the method defined in *Bretherton et al*. [1999]:

$$N_{\text{eff}} = N\frac{1 - r_x r_y}{1 + r_x r_y},$$

where *N* is the total number of available time steps and r_x and r_y are the lag-1 autocorrelations of variables *x* and *y*, respectively.

3. Results

3.1. Observations

Figure 1a shows the spatial map of correlation between the boreal winter (November–March (NDJFM)) SLP anomalies and the Niño3.4 index (defined as the average of SST anomalies over the region 170°–120°W, 5°S–5°N) a year later (i.e., during the following boreal winter). We note that the precursor SLP signal in the

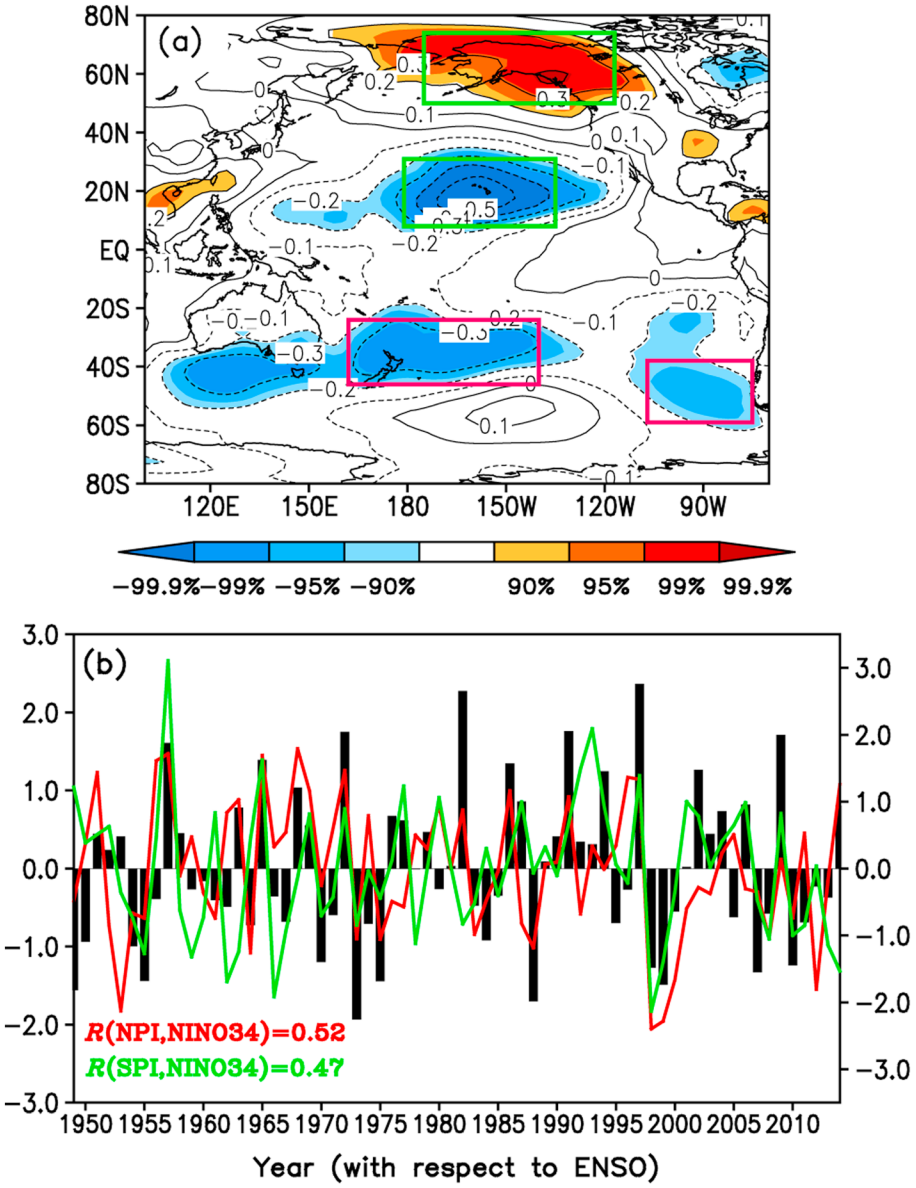

Figure 1. (a) Map of correlation between the boreal winter (November–March (NDJFM)) SLP anomalies and the Niño3.4 index during the following boreal winter. Areas with a correlation significant at or above the 90% confidence level are shaded. The two green boxes (positive correlation box: 175°–117°W, 50°–74°N and negative correlation box: 179°E–135°W, 8°–31°N) are used to define the NPI, and the two magenta boxes with significant negative correlations (from left to right: 162°E–140°W, 46°–24°S and 107°–75°W, 59°–38°S) are used to define the SPI. (b) Time series of the boreal winter NPI (red line) and SPI (green line) overlaid with the Niño3.4 index (black bars) during the following boreal winter. All indices are standardized, and the correlations of the boreal winter NPI and SPI with the Niño3.4 index a year later are given in the lower left corner.

North Pacific shows a pattern similar to the North Pacific Oscillation (NPO) [*Walker and Bliss*, 1932; *Rogers*, 1981], characterized by a north-south dipole pattern of SLP anomalies, whereas the precursor SLP signal in the South Pacific shows a pattern similar to the Pacific-South American (PSA) [*Mo*, 2000], characterized by a wave train extending from the midlatitude southwestern Pacific to the South Pacific near Antarctica and then bending to the southeastern Pacific off the southwest coast of Chile. The NPO and PSA are known as the prominent atmospheric circulation anomaly patterns in the Northern and Southern Hemispheres (NH and SH), respectively. The canonical NPO pattern is generally defined as the second empirical orthogonal function (EOF2) of the seasonal mean SLP anomalies over the North Pacific (120°E–100°W, 15°–80°N) [e.g.,

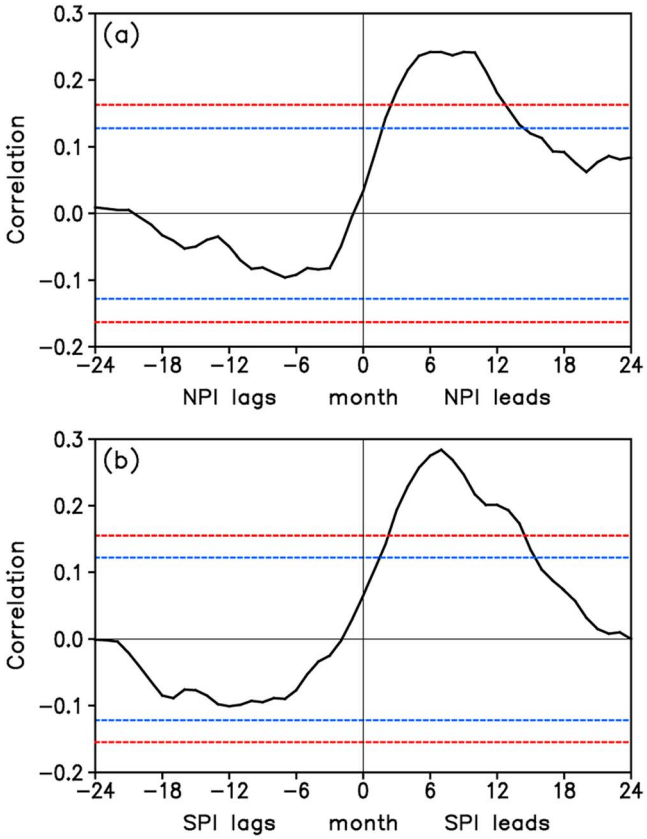

Figure 2. (a) Lead-lag correlations of the monthly (a) NPI and (b) SPI with the monthly Niño3.4 index. In Figures 2a and 2b, the red (blue) horizontal dashed lines indicate the 99.9% (99%) confidence level.

Vimont et al., 2003a]. The second principal component (PC2) time series associated with the EOF2 then defines the time-varying NPO indices. Similarly, the pattern and index of the PSA are usually defined as the EOF2 and PC2 of the seasonal mean SLP anomalies in the SH poleward of 20°S [*Mo*, 2000].

The precursor SLP patterns for ENSO events presented above are consistent with previous findings [e.g., *Vimont et al.*, 2003a, 2003b; *Anderson*, 2003; *Jin and Kirtman*, 2009; *Yu and Kim*, 2011; *Ding et al.*, 2015a, 2015b]. A simple index that measures the variability in the precursor SLP pattern over the North Pacific (hereafter referred to as the North Pacific index, NPI) was constructed by taking the difference of standardized SLP anomalies area averaged over the significant positive and negative correlation centers located in the North Pacific, as indicated in Figure 1a. Similarly, the South Pacific index (SPI) that measures the variability in the precursor SLP pattern over the South Pacific was constructed by taking the sum of standardized SLP anomalies averaged over the two significant negative correlation centers located in the extratropical South Pacific (see Figure 1a). Note that the sign of the SPI is reversed so that the positive SPI is associated with El Niño. The boreal winter NPI exhibits a significant correlation ($R = 0.77$, at the 99.9% confidence level) with the simultaneous NPO index, whereas the boreal winter SPI is significantly correlated with the simultaneous PSA index ($R = 0.51$, at the 99.9% confidence level). The time series of the boreal winter NPI and SPI, overlaid with the Niño3.4 index a year later, are shown in Figure 1b. The correlation of the boreal winter NPI with the Niño3.4 index a year later is 0.52 (significant at the 99.9% confidence level), which is slightly greater than the correlation ($R = 0.47$; also significant at the 99.9% confidence level) of the boreal winter SPI with the Niño3.4 index a year later.

Previous studies have suggested that ENSO can influence the extratropical climate in the North and South Pacific via the so-called atmospheric bridge [e.g., *Lau and Nath*, 1996; *Klein et al.*, 1999; *Alexander et al.*, 2002; *Liu and Alexander*, 2007; *Guan et al.*, 2014a, 2014b]. This leads us to question whether the precursor SLP patterns over the North and South Pacific originate from the tropical Pacific. To address this question, we calculate the lead-lag correlations of the monthly NPI and SPI, respectively, with the monthly Niño3.4 index (Figures 2a and 2b). For lead times of a few months to more than a year, both the NPI and SPI show significant correlations with the Niño3.4 index, with the peak correlations occurring when the NPI (SPI) leads the Niño3.4 index by 6–9 months (~7 months). The simultaneous correlations between the monthly NPI and Niño3.4 index, and between the monthly SPI and Niño3.4 index, are 0.03 and 0.06, respectively, both of which are much lower than their correlations with the Niño3.4 index a few months later. In addition, both the NPI and SPI do not show significant correlations even at the 99% confidence level with the Niño3.4 index when the Niño3.4 index leads the NPI or SPI by more than a few months. Thus, we conclude that the precursor SLP patterns over the North and South Pacific may not simply be a passive response of the North and South Pacific atmosphere to a self-oscillating ENSO cycle; instead, these intrinsic atmospheric variability patterns originating outside the tropical Pacific may make an important contribution to the stochastic forcing of ENSO.

Previous studies have indicated that fluctuations in the boreal winter NPO-like or PSA-like atmospheric pattern can influence the onset and development of ENSO events by changing the wind stress fields over the North or South Pacific, which in turn give rise to a boreal spring SST footprint on the North or South Pacific Ocean [*Vimont et al*., 2003a, 2003b; *Anderson*, 2003; *Wang et al*., 2012; *Ding et al*., 2015a, 2015b] (see also Figure 3). This SST footprint, which is termed the Victoria mode (VM) [*Bond et al*., 2003; *Ding et al*., 2015a] or North Pacific meridional mode (NPMM) [*Chiang and Vimont*, 2004; *Chang et al*., 2007] over the North Pacific and the quadrapole SST mode [*Ding et al*., 2015b] or South Pacific meridional mode [*Zhang et al*., 2014a, 2014b] over the South Pacific, may persist until the boreal summer and can subsequently forces the overlying atmosphere, inducing surface zonal wind anomalies along the equator that are conducive to initiating an ENSO event (the seasonal footprinting mechanism (SFM)) [*Vimont et al*., 2003a, 2003b]. Considering that both the NPI and SPI anomalies influence subsequent ENSO events by modifying the surface zonal wind fields along the equator, the influence of the NPI anomalies on the tropical Pacific might be expected to interfere or interact with the effect of the SPI anomalies.

To test this hypothesis, we explored the joint relationship of the NPI and SPI anomalies to ENSO through scatterplots of the boreal winter (NDJFM) NPI or SPI versus the Niño3.4 index a year later, plotted separately for years in which the NPI and SPI have the same or opposite signs (Figures 4a–4d). We note that the correlation between the boreal winter NPI and the Niño3.4 index a year later is high ($R = 0.68$; significant at the 99.9% confidence level for the 36 events) when the NPI and SPI have the same sign, whereas the correlation is only 0.15 (not significant even at the 90% confidence level for the 30 events) when they have the opposite sign. Likewise, the correlation of the boreal winter SPI with the Niño3.4 index a year later also strongly depends on the NPI: it is 0.66 when the NPI and SPI have the same sign and only 0.08 when they have the opposite sign.

In addition, we compared the strength of the boreal winter Niño3.4 index (represented by its interannual standard deviation (SD)) preceded by the same-sign and opposite-sign NPIs and SPIs and found that the strength of the Niño3.4 index is weaker when the NPI and SPI have the opposite sign in comparison with years in which they have the same sign ($\sigma_{\mathrm{NINO3.4}} = 0.80$ and $\sigma_{\mathrm{NINO3.4}} = 1.23$, respectively; for the full time series $\sigma_{\mathrm{NINO3.4}} = 1.0$ by definition). Furthermore, we compared the percentage of strong, weak, and neutral ENSO events preceded by the same-sign NPI and SPI (Figure 4e). A strong (weak, neutral) ENSO event is defined as a year in which the NDJFM Niño3.4 SST has an intensity greater than 1.0 (0.5–1.0, <0.5) SD of its 1948–2015 time series (Table 1). A high percentage ($>75\%$) of strong ENSO events are preceded by same-sign NPI and SPI. Conversely, only a very low percentage (around 30%) of neutral ENSO events are preceded by same-sign NPI and SPI; instead, around 70% of neutral ENSO events are preceded by opposite-sign NPI and SPI (Figure 4f). These results suggest that when the NPI and SPI are of the opposite sign, the ENSO events following the NPI/SPI anomalies tend to be weaker.

The robustness of the joint impact of the preceding NPI and SPI anomalies on ENSO was validated by repeating similar analyses with two additional reanalysis data sets: the NCEP2 and ERA-Interim. Figures 5a and 5b shows the correlation maps of the boreal winter Niño3.4 index with the previous boreal winter SLP anomalies from the NCEP2 and ERA-Interim data sets, respectively. We note that the NCEP2, ERA-Interim, and NCEP1 (see Figure 1a) data sets show almost identical correlation patterns in the North Pacific poleward of 10°N. The differences among these three data sets mainly lie in the extratropical South Pacific. Compared with the NCEP1, the ERA-Interim and especially NCEP2 show relatively weaker correlations over the southeastern Pacific off the southwest coast of Chile. In addition, significant negative correlations off the east coast of Australia in the NCEP1 data set extend father east than those in the NCEP2 and ERA-Interim data sets. These results are generally consistent with *Bengtsson et al*. [2004] and *Chen et al*. [2008], who reported that due to available observations being more sparse in the SH than in the NH, the reanalysis data are more prone to errors and uncertainties in the SH.

Despite the differences of the precursor SLP patterns for ENSO events among three reanalysis data sets, the NPI/SPI in the NCEP2 and ERA-Interim data sets are defined as SLP anomalies area averaged over the same boxes as those in the NCEP1 data set (Figures 5a and 5b). We explored the joint relationship of the preceding NPI and SPI with the Niño3.4 index in the ERA-Interim and NCEP2 data sets. A significant difference in the correlation of either the boreal winter NPI or SPI with the Niño3.4 index a year later between the same-sign and opposite-sign NPI/SPI years is found in these two additional data sets (Figures 5c–5f), confirming the results obtained above from the NCEP1 data set. It should be pointed out that the focus of this study, the joint relationship between the antecedent North and South Pacific SLP anomalies and ENSO, is not sensitive to the

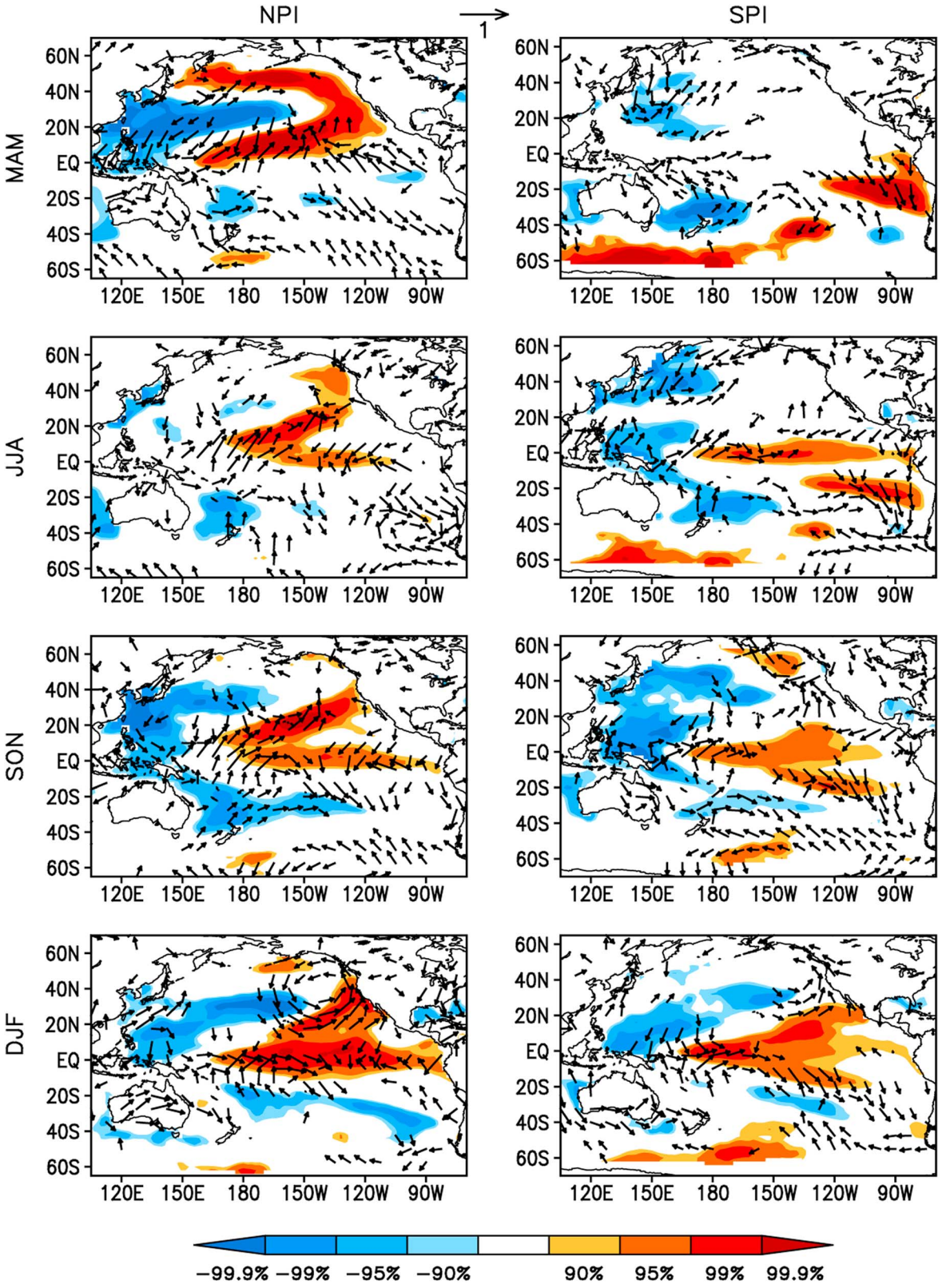

Figure 3. Correlation maps of the December–February (DJF) (left column) NPI and (right column) SPI with the 3 month averaged SST (shading) and surface wind (vectors) anomalies for several lead times (MAM, JJA, September–November (SON), and DJF). The impact of the Niño3.4 index from the previous DJF season was excluded from the 3 month averaged SST and surface wind anomalies using the linear regression method. Positive (red) and negative (blue) SST anomalies with correlations significant at or above the 90% confidence level are shaded. Only surface wind vectors significant at the 90% confidence level are shown.

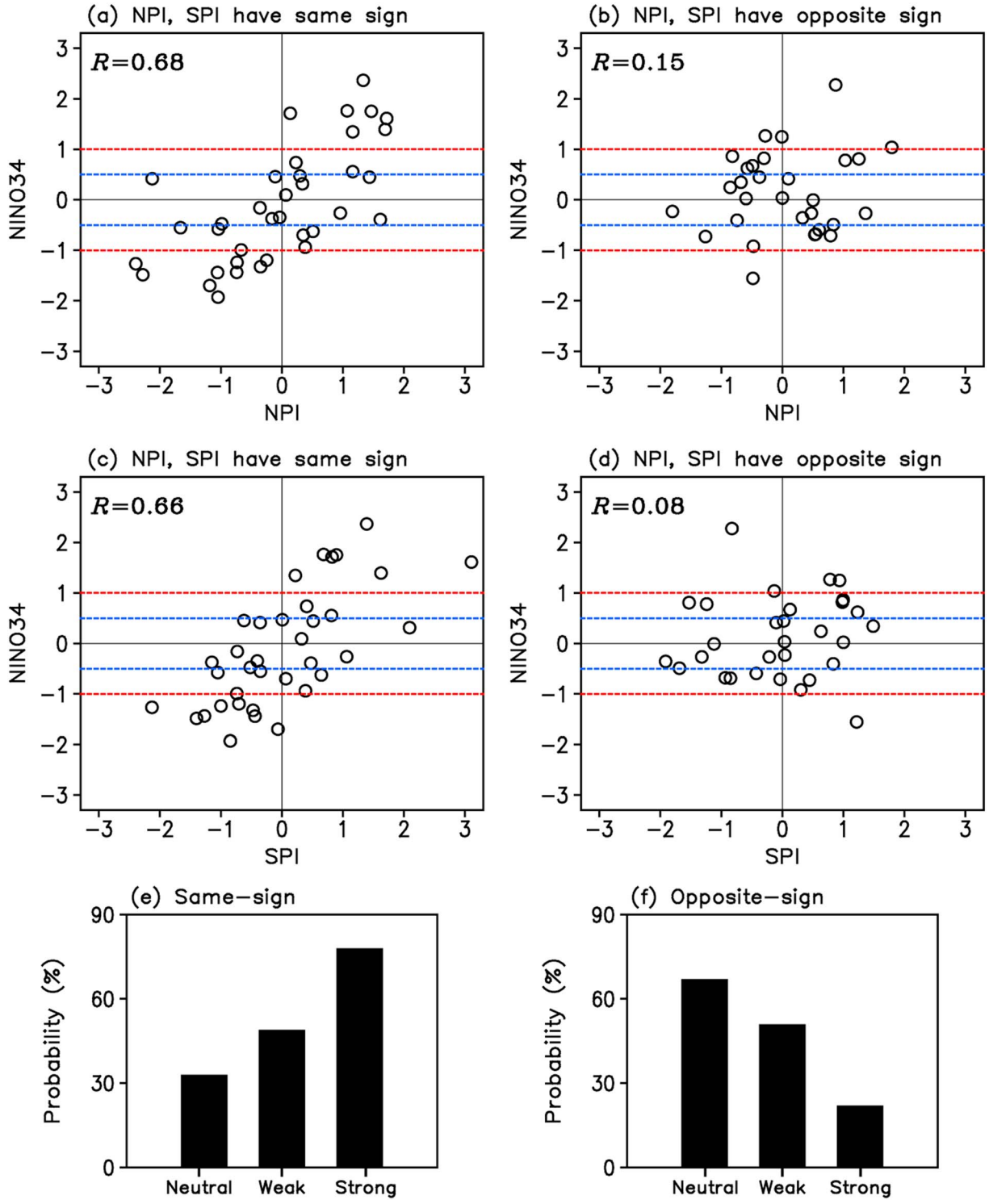

Figure 4. (a) Scatterplot of the boreal winter (NDJFM) NPI versus the Niño3.4 index a year later, plotted only for years in which the NPI has the same sign as the SPI. (b) As for Figure 4a but only for years in which the NPI has the opposite sign to the SPI. (c) Scatterplot of the boreal winter SPI versus the Niño3.4 index a year later, plotted only for years in which the NPI has the same sign as the SPI. (d) As for Figure 4c but only for years in which the NPI has the opposite sign to the SPI. (e) Probability (percentage) of strong, weak, and neutral ENSO events preceded by the same-sign NPI and SPI. (f) As for Figure 4e but for ENSO events preceded by the opposite-sign NPI and SPI. In Figures 4a–4d, the red/blue horizontal dashed lines indicate the boundary of classification of strong (with the standardized Niño3.4 index >1.0), weak (0.5–1.0), and neutral (<0.5) ENSO events.

Table 1. Classification of Strong, Weak, and Neutral ENSO Events During the Period 1948–2015[a]

Strong ENSO	1949, 1955, 1957, 1965, 1968, 1970, 1972, 1973, 1975, 1982, 1986, 1988, 1991, 1994, 1997, 1998, 1999, 2002, 2007, 2009, 2010
Weak ENSO	1950, 1954, 1963, 1964, 1967, 1969, 1971, 1974, 1976, 1977, 1984, 1987, 1995, 2000, 2004, 2005, 2006, 2008, 2011, 2014
Neutral ENSO	1951, 1952, 1953, 1956, 1958, 1959, 1960, 1961, 1962, 1966, 1978, 1979, 1980, 1981, 1983, 1985, 1990, 1992, 1993, 1996, 2001, 2003, 2012, 2013

[a]A strong (weak, neutral) ENSO event is defined as a year in which the NDJFM Niño3.4 SST has an intensity greater than 1.0 (0.5−1.0, <0.5) SD of its 1948–2015 time series.

definition of the NPI or SPI. Similar results can also be obtained in the NCEP2 and ERA-Interim data sets when the NPI (SPI) is defined as SLP anomalies area averaged over only one box region of negative correlation coefficients in the North (South) Pacific (see Figure S1 in the supporting information).

To provide a possible physical interpretation for the joint impact of the preceding NPI and SPI anomalies on ENSO, we show the lagged correlations of the 3 month averaged surface wind and SST anomalies with the December–February (DJF)-averaged NPI of the previous year for years in which the NPI and SPI have the same (left column) and opposite (right column) sign, respectively (Figure 6). To isolate the impacts of the NPI and SPI anomalies on the tropical Pacific climate variability, the ENSO effect (represented by the Niño3.4 index from the previous DJF season) is first removed from the 3 month averaged SST and surface wind anomalies using the linear regression method. For the same-sign NPI/SPI years, an anomalous circulation resembling the NPO generates a marked horseshoe-like SST pattern in the North Pacific during the boreal spring (March–May (MAM)), with a band of positive SST anomalies in the subtropical central-eastern North Pacific extending toward the central equatorial Pacific. At the same time, the NPI-related surface wind anomalies also extend across the entire equatorial Pacific, with the anomalous westerlies over the western-central equatorial Pacific. In addition to anomalous SST anomalies in the North Pacific, significant negative SST anomalies can be clearly seen in the southwestern Pacific. The horseshoe-like SST pattern (primarily its subtropical portion) in the North Pacific persists until the following boreal summer (i.e., June–August (JJA)), which induces the anomalous westerlies over the western-central equatorial Pacific and subsequently results in the development and persistence of anomalous westerlies there. At this time the anomalous southwesterlies generated in response to the significant negative SST anomalies in the southwestern Pacific tend to strengthen the westerly anomalies over the western equatorial Pacific [*Ding et al*., 2015b]. The strengthened westerly anomalies over the western equatorial Pacific in turn are related to the appearance of significant positive SST anomalies in the eastern equatorial Pacific and favor the initiation of an ENSO event [*Bjerknes*, 1969]. In general, the physical process associated with the effects of the NPI anomalies on the equatorial Pacific is slightly different from the SFM proposed by *Vimont et al*. [2003a, 2003b]. The SFM suggests that the NPO-associated extratropical signals propagate into the equatorial Pacific until JJA. However, our analysis indicates that the NPI anomalies affect the surface winds in the equatorial Pacific earlier during MAM.

For the opposite-sign NPI/SPI years, the North Pacific horseshoe-like SST pattern tends to weaken, and its subtropical band of positive SST anomalies does not extend deep enough into the equator during MAM (see Figure 6 (right column)), possibly because of the interference between the NPI- and SPI-related surface wind anomalies over the equatorial Pacific. In the South Pacific, significant negative SST anomalies are no longer evident in the southwestern Pacific but instead occur in the southeastern Pacific during MAM. At the same time, easterly winds strengthen in the eastern equatorial Pacific, which is unfavorable for the development of warm SST anomalies in the region because the stronger winds promote local Ekman upwelling [*Zhu et al*., 2016]. The area-averaged westerly anomalies over the western-central equatorial Pacific for the opposite-sign NPI/SPI years are much weaker than those for the same-sign NPI/SPI years, thereby not favoring the development of ENSO events, as shown in Figure 7. In addition, we also examine the lagged correlations of the 3 month averaged surface wind and SST anomalies with the DJF-averaged SPI of the previous year for years in which the NPI and SPI have the same or opposite signs (supporting information Figure S2). Similarly, the westerly anomalies over the western-central equatorial Pacific for the opposite-sign NPI/SPI years are greatly reduced possibly by the interference between the North and South Pacific surface wind anomalies.

The results presented above indicate that the ability of either the NPI or the SPI to initiate subsequent ENSO events depends on the status of the other index. Furthermore, we note that there is a weak correlation (<0.25) between the boreal winter NPI and SPI time series in Figure 1b, suggesting that the NPI anomalies are relatively independent of the SPI anomalies. Given the relative independence of the NPI and SPI

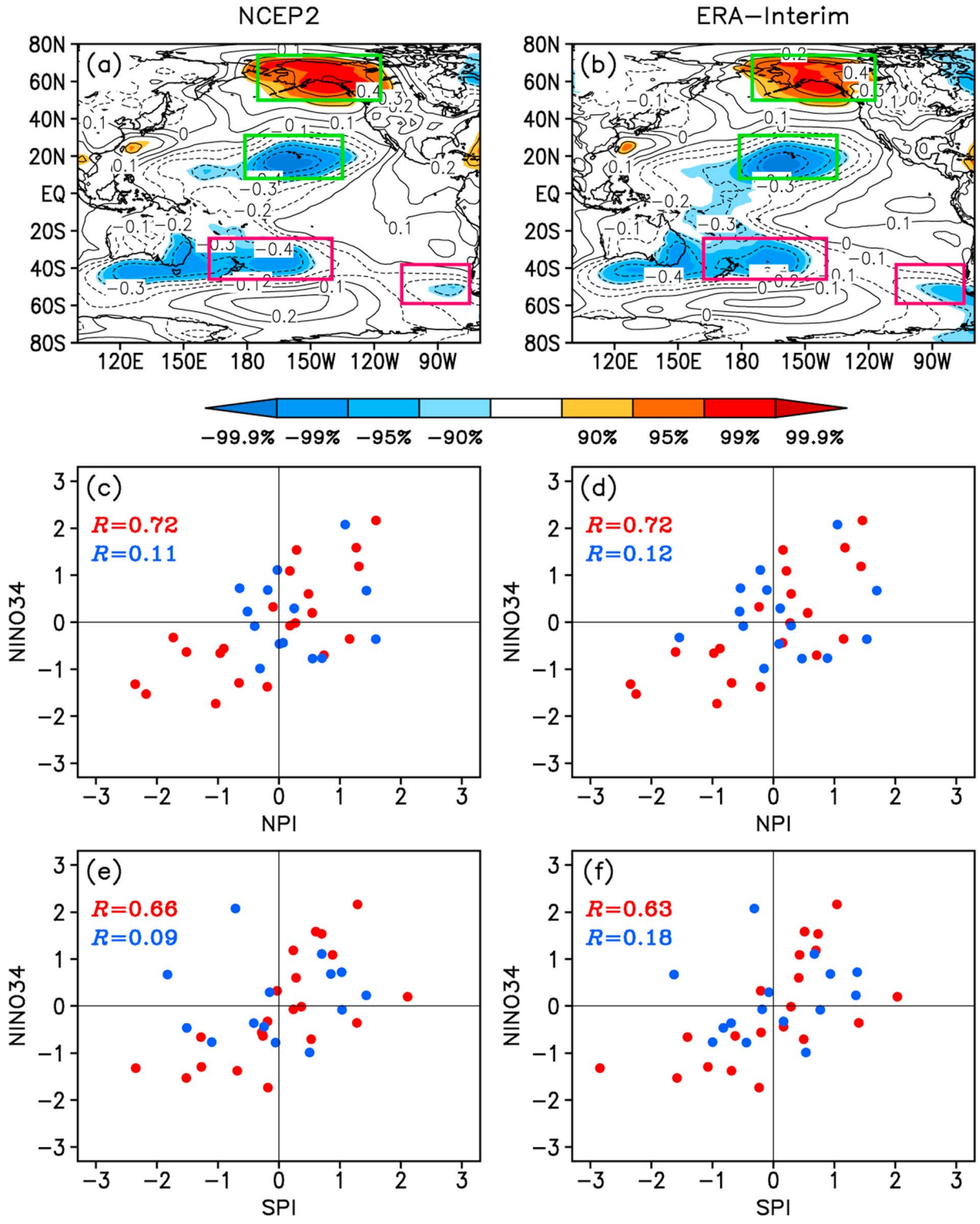

Figure 5. (a) Correlation map of the boreal winter (NDJFM) Niño3.4 index with the previous boreal winter SLP anomalies based on the NCEP2 data set. Areas with a correlation significant at or above the 90% confidence level are shaded. The two green boxes (175°–117°W, 50°–74°N and 179°E–135°W, 8°–31°N) are used to define the NPI, and the magenta box (155°E–150°W, 46°–24°S) is used to define the SPI. (c) Scatterplots of the boreal winter NPI versus the Niño3.4 index a year later. Red (blue) circles indicate the years in which the NPI has the same (opposite) sign as the SPI. Both the NPI and SPI are calculated from the NCEP2 data set. (e) As in Figure 5c but for scatterplots of the boreal winter SPI versus the Niño3.4 index a year later. (b, d, and f) As in Figures 5a, 5c, and 5e, respectively, but for ERA-Interim.

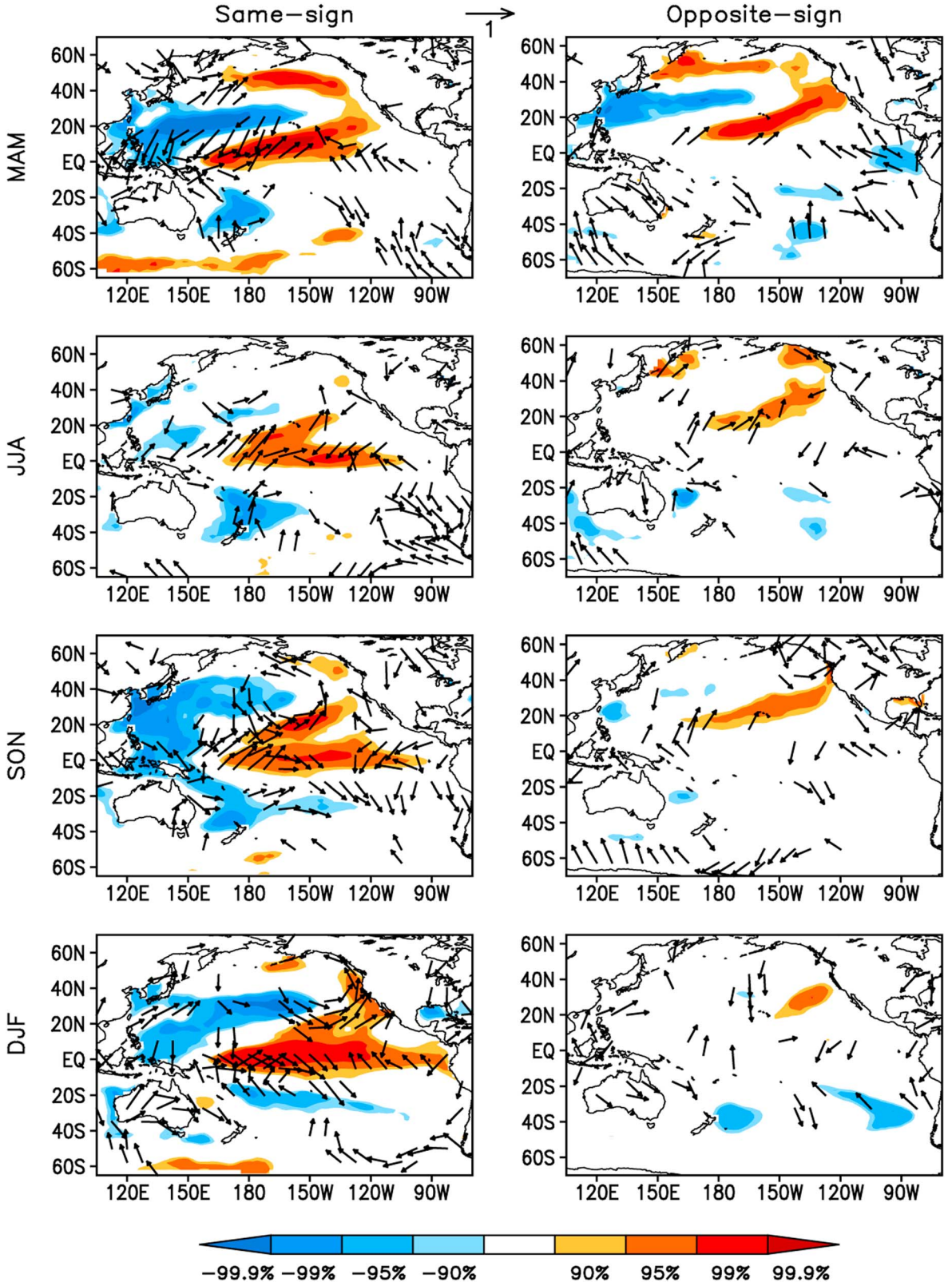

Figure 6. Correlation maps of the 3 month averaged SST (shading) and surface wind (vectors) anomalies with the NPI from the previous DJF season for several lead times (MAM, JJA, SON, and DJF), calculated respectively for years in which the NPI and SPI have the (left column) same and (right column) opposite sign. The impact of the Niño3.4 index from the previous DJF season was excluded from the 3 month averaged SST and surface wind anomalies. Positive (red) and negative (blue) SST anomalies with correlations significant at or above the 90% confidence level are shaded. Only surface wind vectors significant at the 90% confidence level are shown.

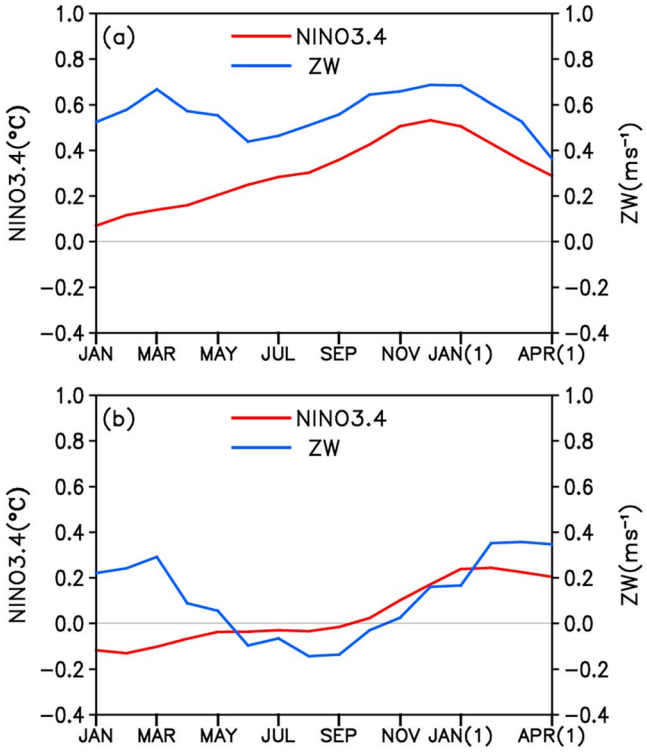

Figure 7. (a) Lagged regressions of the 3 month averaged Niño3.4 index (red line; scale on the left *y* axis) and area-averaged surface zonal wind anomalies over the western-central equatorial Pacific (140°E–170°W, 5°S–5°N) (blue line; scale on the right *y* axis), calculated against the DJF NPI for years in which the NPI and SPI have the same sign. (b) As in Figure 7a but for years in which the NPI and SPI have the opposite sign.

anomalies and their joint relationship with ENSO, an empirical model is established to predict the boreal winter (NDJFM-averaged) Niño3.4 index (referred to as WIN(0)_NINO3.4) based on both the NPI and SPI of the previous boreal winter (referred to as WIN(−1)_NPI and WIN(−1)_SPI, respectively):

$$\begin{aligned}\mathrm{WIN}(0)\_\mathrm{NINO3.4}(t) &= \alpha\times\mathrm{WIN}(-1)\_\mathrm{NPI}(t) \\ &\quad +\beta\times\mathrm{WIN}(-1)\_\mathrm{SPI}(t), \end{aligned} \quad (1)$$

where t is time in years. The performance of the model was cross validated using a leave-one-out scheme (by repeatedly excluding 1 year from the period 1948–2015, determining the coefficients of the linear regression model using the remaining data and then hindcasting the value for the missing year) [*Ham et al.*, 2013; *Ding et al.*, 2015c]. The leave-one-out cross-validation scheme shows that when both the NPI and SPI are applied to hindcast the Niño3.4 index, the cross-validated correlation reaches 0.61, which is higher than using only the NPI ($R = 0.47$) or SPI ($R = 0.42$) to forecast the Niño3.4 index (Figure 8), suggesting that the combined SPI and NPI do provide additional predictability of subsequent ENSO events beyond that associated with the NPI or SPI alone. *Ding et al.* [2015b] developed a similar empirical prediction model of the boreal winter Niño3.4 index, but the model was based on the combined North and South Pacific precursor SST signals (not precursor SLP signals like this study) for ENSO events. Their results also showed that the combined North and South Pacific precursor SST signals provide more useful information than the North or South Pacific precursor SST signal alone for the prediction of subsequent ENSO events.

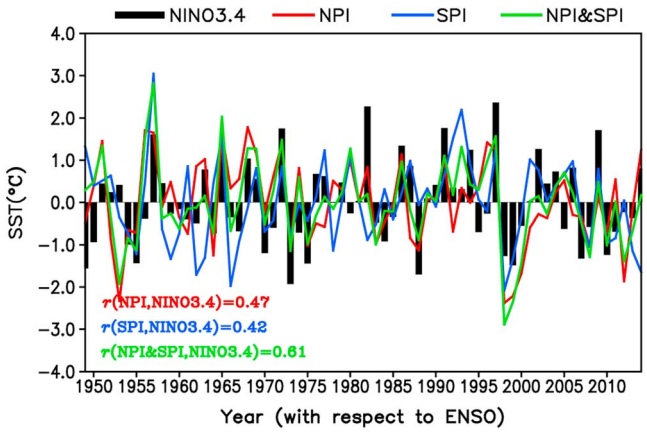

Figure 8. Time series of the observed boreal winter Niño3.4 index (black bars), and the cross-validated hindcasts of the boreal winter Niño3.4 index generated by empirical model (1) using both the combined NPI and SPI (green line), using the NPI alone (red line) and using the SPI alone (blue line). The correlations between various time series are given in the bottom left corner.

3.2. Model Simulations

We first use CESM-LE simulations to evaluate if the current coupled models can reproduce the joint relationship between the tropical Pacific SST anomalies and antecedent North and South Pacific atmospheric variability. Figure 9 shows the correlation maps between the boreal winter (NDJFM) SLP anomalies and the Niño3.4 index (the definition being the same in models and in observations) a year later for the 30 individual CESM-LE members. Almost all

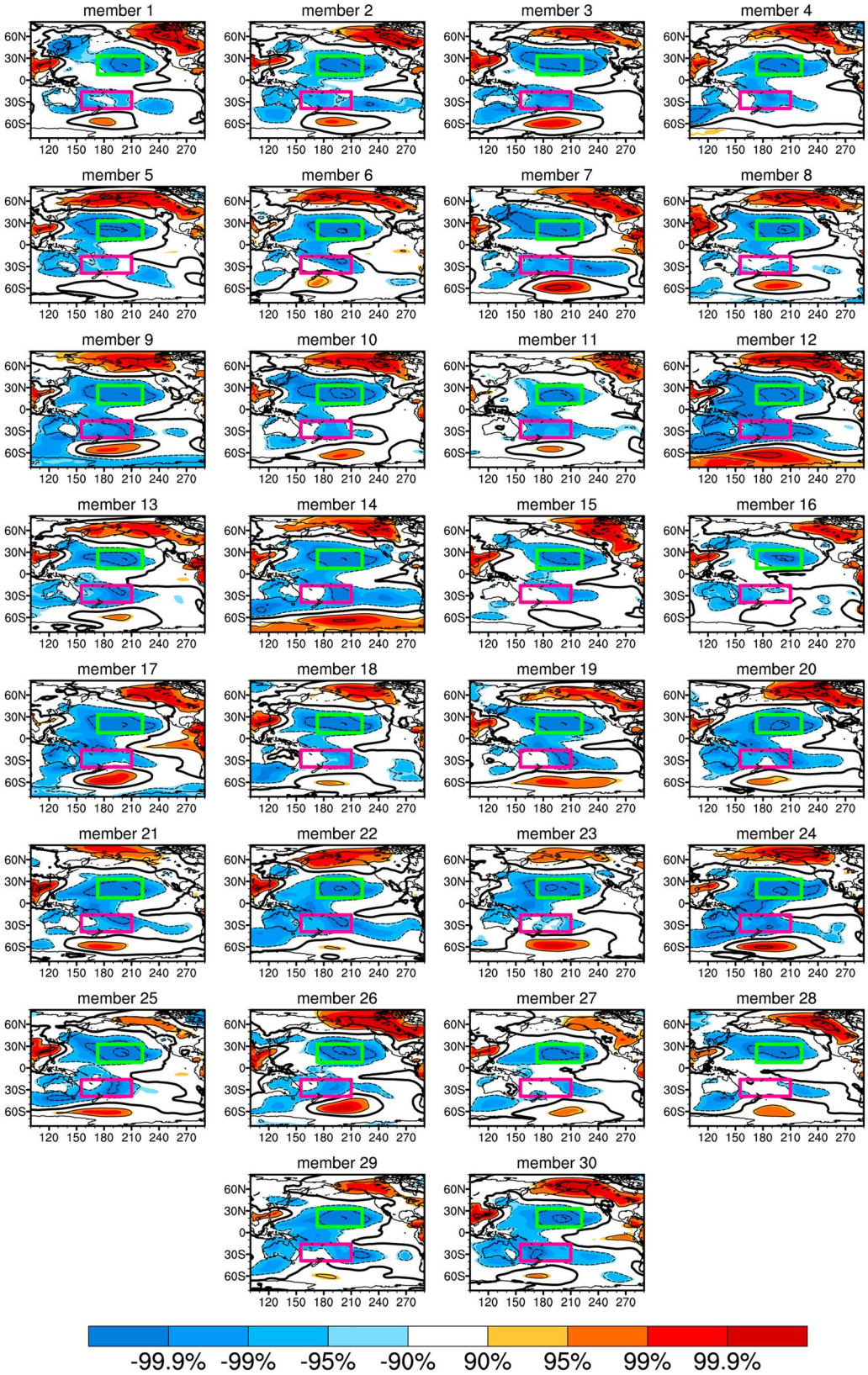

Figure 9. Correlation maps between the boreal winter (NDJFM) SLP anomalies and the Niño3.4 index a year later for the 30 individual CESM-LE members. Areas with a correlation significant at or above the 90% confidence level are shaded. For all members, the green box (173°E–138°W, 8°–33°N) is used to define the NPI, and the magenta box (155°E–150°W, 39°–16°S) is used to define the SPI.

CESM-LE ensemble members show the significant SLP signals over the subtropical and extratropical regions of the North and South Pacific that precede ENSO by 1 year, indicating that the CESM-LE simulations can capture the close connection between boreal winter subtropical and extratropical SLP anomalies over both the North and South Pacific and ENSO a year later. However, there are some differences in the locations of significant positive and negative correlation regions over the North and South Pacific among ensemble members. Specifically, the characteristic dipole pattern of the NPO in the North Pacific is generally captured well by almost all ensemble members but the centers of the northern and southern poles (especially the northern pole) of the NPO do not match spatially well with those of observations (Figures 5a and 5b). In the South Pacific, most CESM-LE ensemble members capture significant negative correlations off the east coast of Australia and positive correlations near Antarctica but do not reproduce significant negative correlations in the southeastern Pacific off the southwest coast of Chile as seen in observations. Given the differences between the observed and simulated precursor SLP patterns of ENSO, the NPI was constructed by only taking the standardized SLP anomalies area averaged over the southern pole of the precursor NPO pattern (173°E–138°W, 8°–33°N). Similarly, the SPI was constructed by only taking the standardized SLP anomalies area averaged over the area off the east coast of Australia (155°E–150°W, 39°–16°S). We note that both these two areas used to define the NPI and SPI show significant negative correlations for almost all CESM-LE ensemble members (Figure 9). The signs of both the NPI and SPI are reversed in CESM-LE simulations.

Figure 10a shows the correlations of the boreal winter (NDJFM) NPI with the Niño3.4 index a year later for the 30 individual CESM-LE members, stratified by whether the NPI has the same or the opposite sign as the SPI (see scatterplots in the supporting information Figure S3). For all CESM-LE ensemble members, the correlations of the boreal winter NPI with the Niño3.4 index a year later are higher when the NPI and SPI have the same sign compared with years in which they have the opposite sign. Likewise, the correlations between the boreal winter SPI and the Niño3.4 index a year later are also strongly influenced by the NPI for all CESM-LE ensemble members (Figure 10b). In addition, for almost all CESM-LE ensemble members (with only one exception occurring in member 27), the strength of the Niño3.4 index is also weaker when the NPI and SPI have the opposite sign in comparison with years in which they have the same sign (Figure 10c). By examining the values of the Niño3.4 index in member 27, we found that there exists one extreme year in which the boreal winter Niño3.4 index reaches 2.92°C when the NPI and SPI have the opposite sign. With the removal of this extreme year, the SD of the boreal winter Niño3.4 index for the opposite-sign NPI/SPI years is reduced from 1.0 to 0.9, and the latter is lower than the SD (0.99) of the Niño3.4 index for the same-sign NPI/SPI years. These results presented above suggest that the interdependence between the North and South Pacific extratropical atmosphere variability in initiating ENSO events can be well represented in CESM-LE.

The above analysis examines the joint relationship between the antecedent North and South Pacific SLP anomalies and ENSO in CESM-LE simulations with externally varying forcings. It further indicates that the SPI anomalies are important for the relationship of the NPI anomalies with ENSO and vice versa. Next, we explore the joint effect of the North and South Pacific atmospheric variability on subsequent ENSO events in the piControl simulations from CESM and CCSM4. Because the external forcing is fixed at the preindustrial level in the piControl simulation, it is possible for us to discuss the role of internal variability alone in the extratropical atmosphere variability-ENSO relationship based on the piControl simulation.

Figure 11a shows the correlation maps between the boreal winter SLP anomalies and the Niño3.4 index a year later in the piControl simulation from CESM. The piControl simulation exhibits generally realistic precursor SLP patterns for ENSO events, characterized by a marked NPO-like pattern over the North Pacific and a PSA-like pattern over the South Pacific that are similar to observations (Figures 5a and 5b). Based on these precursor SLP patterns over the North and South Pacific, we construct the NPI (SLP anomalies area averaged over the box (165°E–138°W, 8°–35°N)) and SPI (SLP anomalies area averaged over the box (155°E–150°W, 39°–16°S)) for the piControl simulation. Note that the boxes used to define the NPI and SPI in the piControl simulation of CESM are very similar to those in CESM-LE simulations (Figure 9).

Scatterplots of the boreal winter NPI and SPI versus the Niño3.4 index a year later in the piControl simulation of CESM, plotted separately for years in which the NPI and SPI have the same or opposite signs, are shown in Figures 11b and 11c, respectively. We can see that the correlation between the NPI and the Niño3.4 index is strongly influenced by the SPI: it is 0.62 and 0.37, respectively, for the same-sign and opposite-sign NPI/SPI years. Likewise, the correlation between the SPI and the Niño3.4 index is substantially different for the

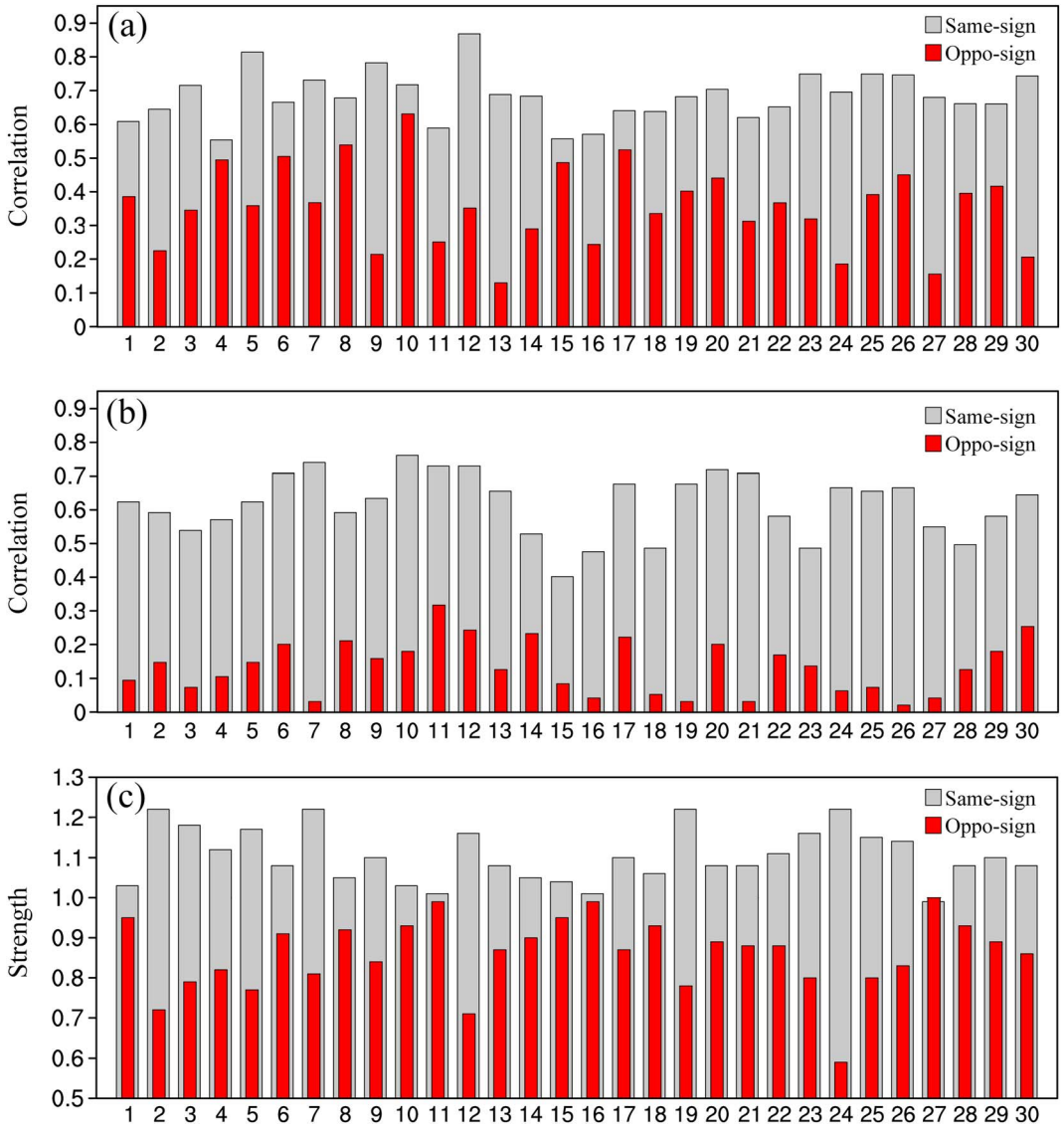

Figure 10. (a) Correlations of the boreal winter (NDJFM) NPI with the Niño3.4 index a year later for the 30 individual CESM-LE members. Gray (red) bars indicate the years in which the NPI has the same (opposite) sign as the SPI. (b) The strength of the boreal winter Niño3.4 index (represented by its interannual standard deviation (SD)) preceded by the same-sign (gray bar) and opposite-sign (red bar) NPIs and SPIs for the 30 individual CESM-LE members.

same-sign and opposite-sign NPI/SPI years (0.59 and 0.01, respectively). Furthermore, a large difference in the strength of the boreal winter Niño3.4 index preceded by the same-sign and opposite-sign NPIs and SPIs is also found in the piControl simulation ($\sigma_{NINO3.4} = 1.08$ and $\sigma_{NINO3.4} = 0.91$, respectively). Similar results can also be obtained for the piControl simulation of CCSM4 in which the correlation between the boreal winter NPI (SPI) and the Niño3.4 index a year later is 0.64 and 0.18 (0.59 and 0.09), respectively, for the same-sign and opposite-sign NPI/SPI years (Figure 12), and the SD of the boreal winter Niño3.4 index preceded by the same-sign and opposite-sign NPIs and SPIs is 1.11 and 0.84, respectively. These results from both the CESM and CCSM4 piControl simulations are very similar to those from observations and CESM-LE simulations, which provide further evidence of the joint role of atmospheric circulation precursors over the North and South Pacific in initiating ENSO. These results also suggest that interval variability may play a dominant role in the extratropical atmosphere variability-ENSO relationship, considering the piControl simulation without externally varying forcings. It is speculated that this joint relationship between the North/South Pacific extratropical atmosphere variability and ENSO may not change significantly under future climate conditions. Further research is necessary to verify this speculation by analyzing

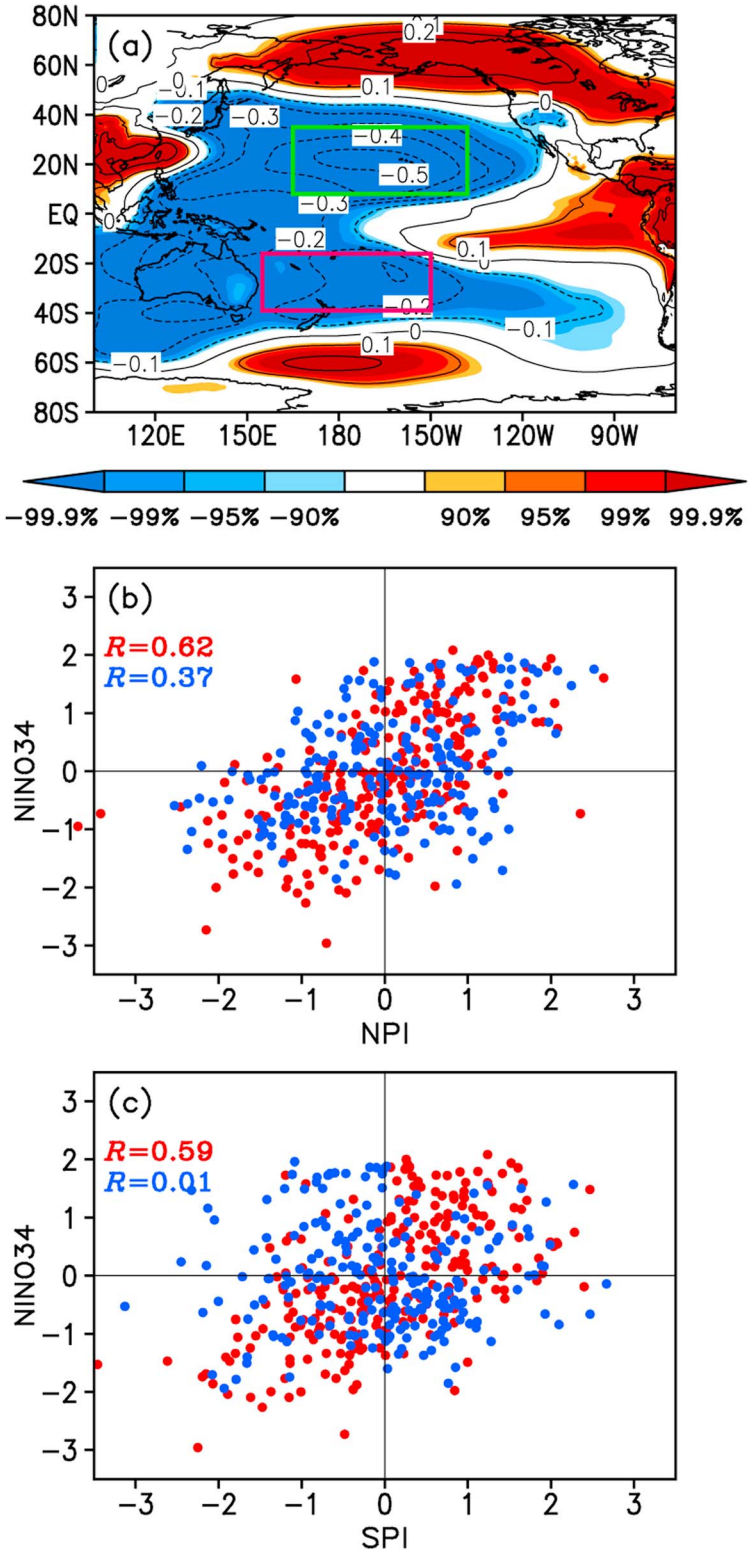

Figure 11. (a) Correlation maps between the boreal winter (NDJFM) SLP anomalies and the Niño3.4 index a year later in the 501 year piControl experiment of CESM. Areas with a correlation significant at or above the 90% confidence level are shaded. The green box (165°E–138°W, 8°–35°N) is used to define the NPI, and the magenta box (155°E–150°W, 39°–16°S) is used to define the SPI. (b) Scatterplots of the boreal winter NPI versus the Niño3.4 index a year later. Red (blue) circles indicate the years in which the NPI has the same (opposite) sign as the SPI. (c) As in 11b but for scatterplots of the boreal winter SPI versus the Niño3.4 index a year later.

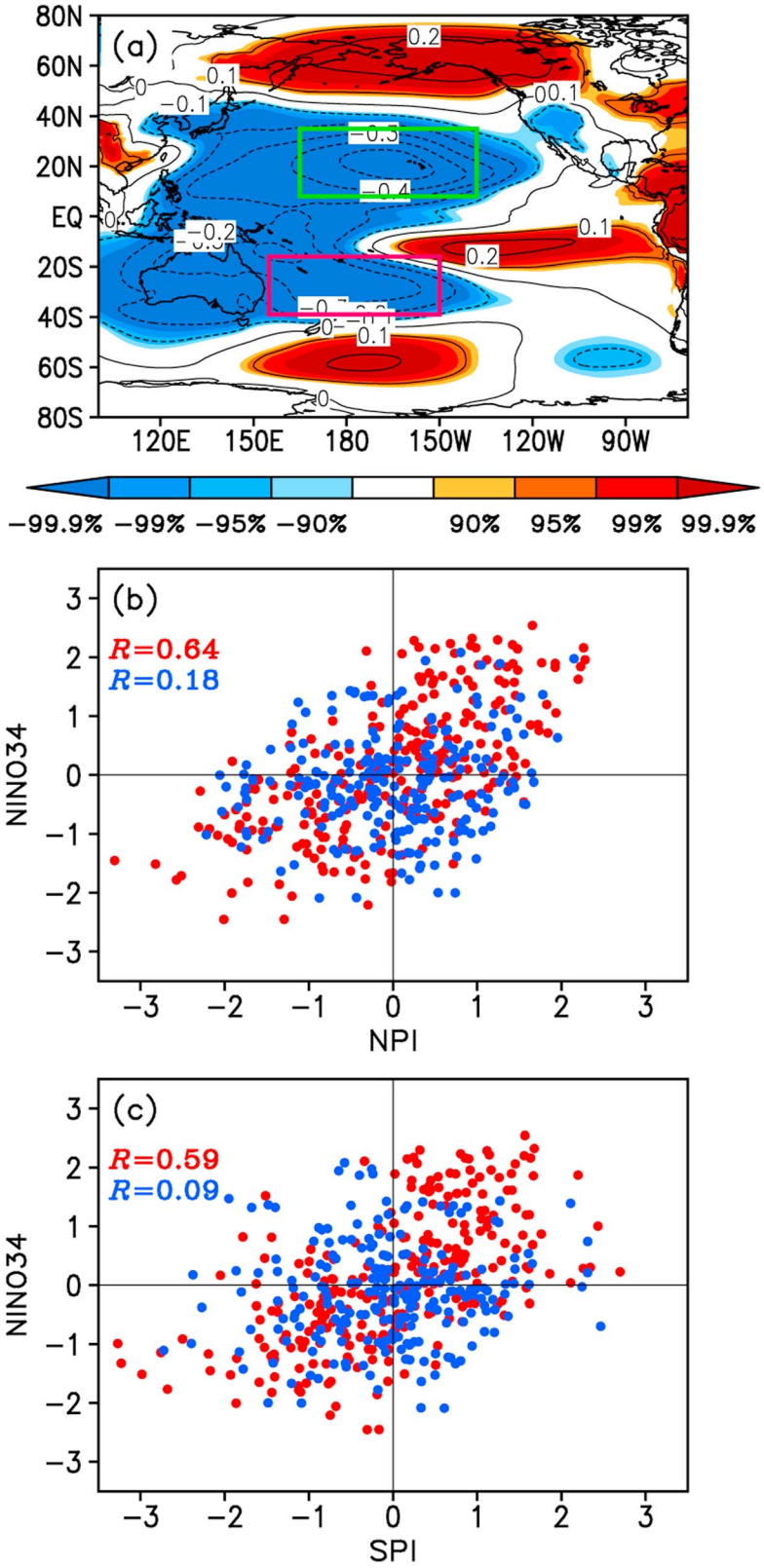

Figure 12. As in Figure 11 but for (a) correlation maps between the boreal winter SLP anomalies and the Niño3.4 index a year later and (b and c) scatterplots of the boreal winter NPI/SPI versus the Niño3.4 index a year later in the 501 year piControl experiment of CCSM4. The boxes used to define the NPI and SPI in the piControl simulation of CCSM4 are same as those in the piControl simulation of CESM.

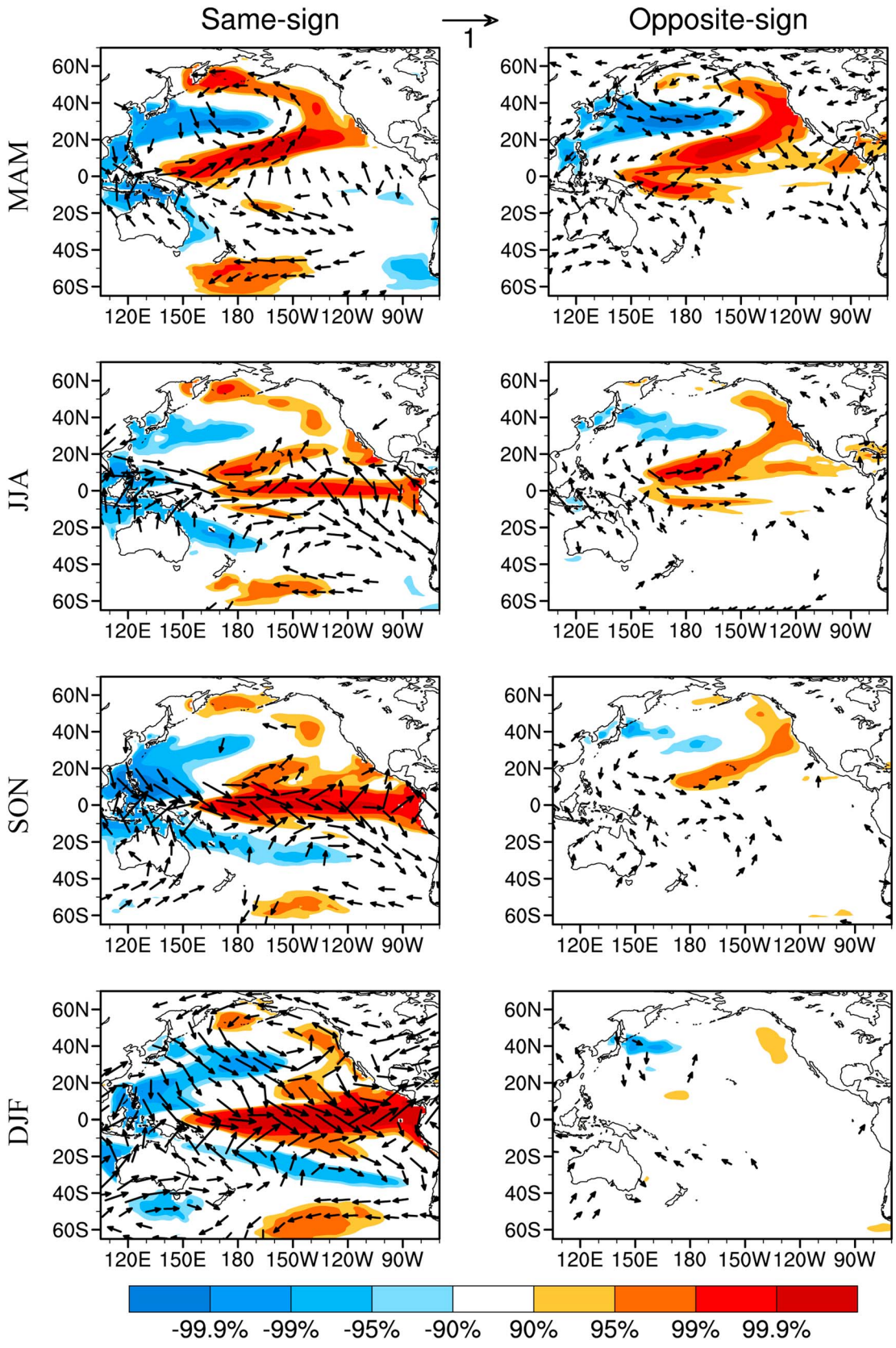

Figure 13. As in Figure 6 but for correlation maps of the 3 month averaged SST (shading) and surface wind (vectors) anomalies with the NPI from the previous DJF season for several lead times in the piControl simulation of CCSM4.

the historical and future climate simulations in phase 5 of the Coupled Model Intercomparison Project (CMIP5) [*Taylor et al.*, 2012].

The evolutions of the 3 month averaged NPI-related surface wind and SST anomalies for years in which the NPI and SPI have the same and opposite sign are also evaluated in the piControl simulation of CCSM4 (Figure 13). For the same-sign NPI/SPI years, the horseshoe-like SST pattern in the North Pacific and significant negative SST anomalies off the east coast of Australia are clearly seen during the boreal spring (MAM). These SST anomalies persist until the following boreal summer (i.e., JJA) and subsequently induce the anomalous westerlies over the western equatorial Pacific, strengthening the latter and thereby leading to the development of positive SST anomalies in the eastern equatorial Pacific. In contrast, for the opposite-sign NPI/SPI years in the piControl simulation, anomalous SST anomalies in the South Pacific becomes indistinct during MAM, which might hinder the development of the anomalous westerlies over the western equatorial Pacific during the following boreal summer and hence the initiation of ENSO events. These results suggest that the processes in the North Pacific involved in initiating ENSO events for both the same-sign and opposite-sign NPI/SPI years in the CCSM4 piControl simulation are generally similar to those in observations and strongly depend on the state of the South Pacific.

4. Summary and Discussion

This study examined the joint relationship of the subtropical/extratropical precursor SLP anomalies over the North and South Pacific with the onset of ENSO events. We have found that the relationship of the North Pacific precursor SLP anomalies to the onset of subsequent ENSO events may strongly depend on the state of the simultaneous South Pacific precursor SLP anomalies and vice versa. When the boreal winter subtropical/extratropical SLP anomalies over the North and South Pacific have the opposite sign, the correlation of the North Pacific or South Pacific anomalies with the subsequent ENSO state becomes much smaller, and the strength of the ENSO events also tends to be weaker. One possible reason for this is that the westerly anomalies over the western-central equatorial Pacific during the following boreal summer are greatly reduced by the interference between the antecedent North and South Pacific SLP anomalies, thereby not favoring the development of ENSO events. The relative independence of the precursor SLP anomalies over the North and South Pacific leads us to speculate that their fluctuations may work together to be useful predictors of ENSO events. Thus, we developed an empirical model to hindcast the boreal winter Niño3.4 index using a combination of two indices that are derived from the previous boreal winter North and South Pacific SLP anomalies. The results indicate that the model does have the potential to improve the ENSO prediction skill with a lead time of up to 1 year.

The modeled results from the CESM-LE confirm that the North Pacific precursor SLP anomalies influence on ENSO interferes with the impact of the South Pacific precursor SLP anomalies. This joint impact of North and South Pacific atmospheric variability on the onset of ENSO events is a robust feature of the CESM-LE and appears in all ensemble members. In addition, the joint relationship between the tropical Pacific SST anomalies and antecedent North and South Pacific atmospheric variability can be well reproduced in the piControl simulations of CESM and CCSM4 without externally varying forcings, suggesting that the extratropical atmosphere variability-ENSO relationship is not sensitive to changes in external forcings.

It should be noted that 2014 was a typical year in which the NPI and SPI in the previous boreal winter showed large-amplitude anomalies of the opposite sign (1.25 and −1.53, respectively; see Figure 1b). At the beginning of 2014, many climate scientists [*Glantz*, 2015], and most climate models [http://iri.columbia.edu/our-expertise/climate/forecasts/enso/2014-April-quick-look], predicted the occurrence of a super El Niño, comparable with the 1997/1998 event, in the subsequent boreal winter. However, the 2014 event did not develop as expected and turned out to be a weak El Niño event. Considerable attention has been devoted to understanding the reasons for this. *Menkes et al.* [2014] and *Chen et al.* [2015] emphasized the effects of WWEs, whereas *Min et al.* [2015] and *Zhu et al.* [2016] argued that the abrupt termination of the 2014 warming was caused primarily by negative SST anomalies in the southeastern Pacific. In view of the combined effect of the NPI and SPI anomalies on the subsequent ENSO events presented above, we speculate that the absence of a super El Niño in 2014 can be attributed, at least in part, to the opposite-sign NPI and SPI anomalies in the previous boreal winter. As shown in Figure 6, opposite-sign NPI and SPI anomalies are associated with anomalous SSTs in the southeastern Pacific and weakened westerly anomalies (presumably associated

with the suppression of WWEs) in the western equatorial Pacific during MAM, which tend to favor a weaker El Niño in the subsequent boreal winter. At this point, our results are generally consistent with those of previous studies [*Menkes et al*., 2014; *Chen et al*., 2015; *Min et al*., 2015; *Zhu et al*., 2016].

In addition, although ENSO predictions have made remarkable progress over the past three decades, they are still hampered by the boreal spring predictability barrier [*Webster and Yang*, 1992; *Torrence and Webster*, 1998]. Our results suggest that the boreal winter subtropical/extratropical precursor fields over the North and South Pacific can together have a great influence on the onset of ENSO events. Thus, the combination of North and South Pacific precursor fields may be a good candidate for ENSO predictions across the boreal spring. We speculate that if the joint relationship of the North and South Pacific precursor fields with the onset of ENSO events could be captured satisfactorily by the forecast models, this may lead to a significant improvement in ENSO predictions across the boreal spring. An assessment of the real predictive use of the North and South Pacific precursor SLP signals as a supplemental tool for the prediction of ENSO events within a forecast framework is currently underway. In addition, *Anderson* [2007] suggested that the processes of the North Pacific subtropical SLP anomalies in initiating ENSO also strongly depend on the state of the tropical Pacific. When the subtropical SLP anomalies over the central North Pacific and the heat content anomalies in the western equatorial Pacific have the same sign, their impact on ENSO is much weaker. Additional analysis of the joint impact of the tropical and extratropical precursors on the onset of ENSO would also be worthwhile.

Acknowledgments

Q. R. Ding and C. Sun are supported by CMA Project (GYHY201506013), NSFC grant (41522502), and CAS Project (XDA11010303). The NCEP1 and NCEP2 data sets are available from http://www.esrl.noaa.gov/psd/data/gridded/. The ERA-Interim data set is available from http://apps.ecmwf.int/datasets/data/interim-full-daily/levtype=sfc/. The ERSSTv3b data set is obtained from http://www.esrl.noaa.gov/psd/data/gridded/data.noaa.ersst.v3.html. We acknowledge the CESM-LE project for producing and making available model outputs (http://www.cesm.ucar.edu/projects/community-projects/LENS/data-sets.html). The CCSM4 piControl simulation data used in this study are available from the Coupled Model Intercomparison Project Phase 5 (CMIP5) at http://cmip-pcmdi.llnl.gov/cmip5/data_portal.html.

References

Alexander, M. A., I. Bladé, M. Newman, J. R. Lanzante, N. C. Lau, and J. D. Scott (2002), The atmospheric bridge: The influence of ENSO teleconnections on air–sea interaction over the global oceans, *J. Clim.*, *15*, 2205–2231.

Alexander, M. A., D. J. Vimont, P. Chang, and J. D. Scott (2010), The impact of extratropical atmospheric variability on ENSO: Testing the seasonal footprinting mechanism using coupled model experiments, *J. Clim.*, *23*, 2885–2901.

Anderson, B. T. (2003), Tropical Pacific sea-surface temperatures and preceding sea level pressure anomalies in the subtropical North Pacific, *J. Geophys. Res.*, *108*(D23), 4732, doi:10.1029/2003JD003805.

Anderson, B. T. (2007), On the joint role of subtropical atmospheric variability and equatorial subsurface heat content anomalies in initiating the onset of ENSO events, *J. Clim.*, *20*, 1593–1599.

Anderson, B. T., and E. Maloney (2006), Interannual tropical Pacific sea surface temperatures and their relation to preceding sea level pressures in the NCAR CCSM2, *J. Clim.*, *19*, 998–1012.

Bengtsson, L., S. Hagemann, and K. I. Hodges (2004), Can climate trends be calculated from reanalysis data?, *J. Geophys. Res.*, *109*, D11111, doi:10.1029/2004JD004536.

Bjerknes, J. (1969), Atmospheric teleconnections from the equatorial Pacific, *Mon. Weather Rev.*, *97*, 163–172.

Bond, N. A., J. E. Overland, M. Spillane, and P. Stabeno (2003), Recent shifts in the state of the North Pacific, *Geophys. Res. Lett.*, *30*(23), 2183, doi:10.1029/2003GL018597.

Bretherton, C. S., M. Widmann, V. P. Dymnidov, J. M. Wallace, and I. Blade (1999), The effective number of spatial degrees of freedom of a time-varying field, *J. Clim.*, *12*, 1990–2009.

Chang, P., L. Zhang, R. Saravanan, D. J. Vimont, J. C. H. Chiang, L. Ji, H. Seidel, and M. K. Tippett (2007), Pacific meridional mode and El Niño–Southern Oscillation, *Geophys. Res. Lett.*, *34*, L16608, doi:10.1029/2007GL030302.

Chen, D. K., T. Lian, C. B. Fu, M. A. Cane, Y. M. Tang, R. Murtugudde, X. S. Song, Q. Y. Wu, and L. Zhou (2015), Strong influence of westerly wind bursts on El Niño diversity, *Nat. Geosci.*, *8*, 339–345, doi:10.1038/NGEO2399.

Chen, J., A. D. DelGenio, B. E. Carlson, and M. G. Bosilovich (2008), The spatiotemporal structure of twentieth-century climate variations in observations and reanalyses. Part I: long-term trend, *J. Clim.*, *21*, 2611–2633.

Chiang, J., and D. J. Vimont (2004), Analogous Pacific and Atlantic meridional modes of tropical atmosphere–ocean variability, *J. Clim.*, *17*, 4143–4158.

Danabasoglu, G., S. G. Yeager, Y.-O. Kwon, J. J. Tribbia, A. S. Phillips, and J. W. Hurrell (2012), Variability of the Atlantic meridional overturning circulation in CCSM4, *J. Clim.*, *25*, 5153–5172.

Dee, D. P., et al. (2011), The ERA-Interim reanalysis: configuration and performance of the data assimilation system, *Quart. J. Roy. Meteor. Soc.*, *137*, 553–597.

Ding, R. Q., J. P. Li, Y.-H. Tseng, C. Sun, and Y. P. Guo (2015a), The Victoria mode in the North Pacific linking extratropical sea level pressure variations to ENSO, *J. Geophys. Res. Atmos.*, *120*, 27–45, doi:10.1002/2014JD022221.

Ding, R. Q., J. P. Li, and Y.-H. Tseng (2015b), The impact of South Pacific extratropical forcing on ENSO and comparisons with the North Pacific, *Clim. Dyn.*, *44*, 2017–2034, doi:10.1007/s00382-014-2303-5.

Ding, R. Q., J. P. Li, Y.-H. Tseng, and Q. C. Ruan (2015c), Influence of the North Pacific Victoria mode on the Pacific ITCZ summer precipitation, *J. Geophys. Res. Atmos.*, *120*, 964–979, doi:10.1002/2014JD022364.

Gent, P. R., et al. (2011), The Community Climate System Model version 4, *J. Clim.*, *24*, 4973–4991.

Glantz, M. H. (2015), Shades of chaos: Lessons learned about lessons learned about forecasting El Niño and its impacts, *Int. J. Disaster Risk Sci.*, *6*, 94–103.

Guan, Y., J. Zhu, B. Huang, Z.-Z. Hu, and J. L. Kinter III (2014a), South Pacific Ocean dipole: A predictable mode on multiseasonal time scales, *J. Clim.*, *27*, 1648–1658.

Guan, Y., B. Huang, J. Zhu, Z.-Z. Hu, and J. L. Kinter III (2014b), Interannual variability of the South Pacific Ocean in observations and simulated by the NCEP Climate Forecast System, version 2, *Clim. Dyn.*, *43*, 1141–1157.

Ham, Y.-G., J.-S. Kug, and J.-Y. Park (2013), Two distinct roles of Atlantic SSTs in ENSO variability: North Tropical Atlantic SST and Atlantic Niño, *Geophys. Res. Lett.*, *40*, 4012–4017, doi:10.1002/grl.50729.

Hong, L.-C., LinHo, and F.-F. Jin (2014), A Southern Hemisphere booster of super El Niño, *Geophys. Res. Lett.*, *41*, 2142–2149, doi:10.1002/2014GL059370.
Jin, D., and B. P. Kirtman (2009) Why the Southern Hemisphere ENSO responses lead ENSO?, *J. Geophys. Res.*, *114*, D23101, doi:10.1029/2009JD012657.
Kalnay, E., et al. (1996), The NCEP–NCAR 40-Year Reanalysis Project, *Bull. Am. Meteorol. Soc.*, *77*, 437–471.
Kanamitsu, M., W. Ebisuzaki, J. Woollen, S.-K. Yang, J. J. Hnilo, M. Fiorino, and G. L. Potter (2002), NCEP-DOE AMIP-II Reanalysis (R-2), *Bull. Am. Meteorol. Soc.*, *83*, 1631–1643.
Kay, J. E., et al. (2015), The Community Earth System Model (CESM) large ensemble project: A community resource for studying climate change in the presence of internal climate variability, *Bull. Am. Meteorol. Soc.*, *96*, 1333–1349.
Klein, S. A., B. J. Soden, and N.-C. Lau (1999), Remote sea surface temperature variations during ENSO: Evidence for a tropical atmospheric bridge, *J. Clim.*, *12*, 917–932.
Larson, S. M., and B. P. Kirtman (2014), The Pacific meridional mode as an ENSO precursor and predictor in the North American multimodel ensemble, *J. Clim.*, *12*, 917–932.
Lau, N.-C., and M. J. Nath (1996), The role of the "atmospheric bridge" in linking tropical Pacific ENSO events to extratropical SST anomalies, *J. Clim.*, *9*, 2036–2057.
Liu, Z., and M. Alexander (2007) Atmospheric bridge, oceanic tunnel, and global climatic teleconnections, *Rev. Geophys.*, *45*, RG2005, doi:10.1029/2005RG000172.
Madden, R. A., and P. R. Julian (1994), Observations of the 40–50-day tropical oscillation—A review, *Mon. Weather Rev.*, *122*, 814−837.
Menkes, C. E., M. Lengaigne, J. Vialard, M. Puy, P. Marchesiello, S. Cravatte, and G. Cambon (2014), About the role of Westerly Wind Events in the possible development of an El Niño in 2014, *Geophys. Res. Lett.*, *41*, 6476–6483, doi:10.1002/2014GL061186.
McPhaden, M. J., F. Bahr, Y. D. Penhoat, E. Firing, S. P. Hayes, P. P. Niiler, P. L. Richardson, and J. M. Toole (1992), The response of the western equatorial Pacific Ocean to westerly wind bursts during November 1989 to January 1990, *J. Geophys. Res.*, *97*, 14,289–14,303, doi:10.1029/92JC01197.
Min, Q., J. Su, R. Zhang, and X. Rong (2015), What hindered the El Niño pattern in 2014?, *Geophys. Res. Lett.*, *42*, 6762–6770, doi:10.1002/2015GL064899.
Mo, K. C. (2000), Relationships between low-frequency variability in the Southern Hemisphere and sea surface temperature anomalies, *J. Clim.*, *13*, 3599–3610.
McPhaden, M. J. (1999), Genesis and evolution of the 1997–98 El Niño, *Science*, *283*, 950–954, doi:10.1126/science.283.5404.950.
Rogers, J. C. (1981), The North Pacific Oscillation, *J. Clim.*, *1*, 39–57.
Smith, T. M., R. W. Reynolds, T. C. Peterson, and J. Lawrimore (2008), Improvements to NOAA's historical merged land-ocean surface temperature analysis (1880–2006), *J. Clim.*, *21*, 2283–2296.
Taylor, K. E., R. J. Stouffer, and G. A. Meehl (2012), An overview of CMIP5 and the experiment design, *Bull. Am. Meteorol. Soc.*, *93*, 485–498.
Terray, P. (2011), Southern Hemisphere extra-tropical forcing: a new paradigm for El Niño–Southern Oscillation, *Clim. Dyn.*, *36*, 2171–2199.
Torrence, C., and P. J. Webster (1998), The annual cycle of persistence in the El Niño/Southern Oscillation, *Quart. J. Roy. Meteor. Soc.*, *124*, 1985–2004, doi:10.1002/qj.49712455010.
Vimont, D. J., J. M. Wallace, and D. S. Battisti (2003a), The seasonal footprinting mechanism in the Pacific: Implications for ENSO, *J. Clim.*, *16*, 2668–2675.
Vimont, D. J., D. S. Battisti, and A. C. Hirst (2003b), The seasonal footprinting mechanism in the CSIRO general circulation models, *J. Clim.*, *16*, 2653–2667.
Vimont, D. J., M. Alexander, and A. Fontaine (2009), Midlatitude excitation of tropical variability in the Pacific: The role of thermodynamic coupling and seasonality, *J. Clim.*, *22*, 518–534.
Walker, G. T., and E. W. Bliss (1932), World weather V, *Mem. Roy. Meteor. Soc.*, *4*, 53–84.
Wang, S.-Y., M. L'Heureux, and H.-H. Chia (2012), ENSO prediction one year in advance using western North Pacific sea surface temperatures, *Geophys. Res. Lett.*, *39*, L05702, doi:10.1029/2012GL050909.
Webster, P. J., and S. Yang (1992), Monsoon and ENSO: Selectively interactive systems, *Q. J. R. Meteorol. Soc.*, *118*, 877−926, doi:10.1002/qj.49711850705.
Yu, J.-Y., and S.-T. Kim (2011), Relationships between extratropical sea level pressure variations and the central Pacific and eastern Pacific types of ENSO, *J. Clim.*, *24*, 708–720.
Yu, J.-Y., H.-Y. Kao, and T. Lee (2010), Subtropics-related interannual sea surface temperature variability in the central equatorial Pacific, *J. Clim.*, *23*, 2869–2884.
Zhang, H., A. Clement, and P. Di Nezio (2014a), The South Pacific meridional mode: A mechanism for ENSO-like variability, *J. Clim.*, *10*, 769–783.
Zhang, H., C. Deser, A. Clement, and R. Tomas (2014b), Equatorial signatures of the Pacific Meridional Modes: Dependence on mean climate state, *Geophys. Res. Lett.*, *41*, 568–574, doi:10.1002/2013GL058842.
Zhu, J. S., A. Kumar, B. H. Huang, M. A. Balmaseda, Z.-Z. Hu, L. Marx, and J. L. Kinter III (2016), The role of off-equatorial surface temperature anomalies in the 2014 El Niño prediction, *Sci. Repts.*, *6*, 19677, doi:10.1038/srep19677.